

Solutions of the 1D Coupled Nonlinear Schrödinger Equations by the CIP-BS Method

Takayuki Utsumi^{1,*}, Takayuki Aoki², James Koga³ and Mitsuru Yamagiwa³

¹ *Department of Electronics and Computer Science, Tokyo University of Science, Yamaguchi, 1-1 Daigaku-dori, Sanyou-Onoda, Yamaguchi 756-0884, Japan.*

² *Global Scientific Information and Computing Center, Tokyo Institute of Technology, O-okayama, Meguro-ku, Tokyo 152-8552, Japan.*

³ *Japan Atomic Energy Agency, 8-1 Umemidai Kizu-cho, Souraku-gun, Kyoto 619-0215, Japan.*

Received 30 August 2005; Accepted (in revised version) 25 November 2005

Communicated by Takashi Yabe

Abstract. In this paper, we present solutions for the one-dimensional coupled nonlinear Schrödinger (CNLS) equations by the Constrained Interpolation Profile - Basis Set (CIP-BS) method. This method uses a simple polynomial basis set, by which physical quantities are approximated with their values and derivatives associated with grid points. Nonlinear operations on functions are carried out in the framework of differential algebra. Then, by introducing scalar products and requiring the residue to be orthogonal to the basis, the linear and nonlinear partial differential equations are reduced to ordinary differential equations for values and spatial derivatives. The method gives stable, less diffusive, and accurate results for the CNLS equations.

Key words: The CIP-BS method; basis set; differential algebra; the Galerkin method; the coupled nonlinear Schrödinger equation.

1 Introduction

In 1965, the numerical experiment of Zabusky and Kruskal [1] initiated the development of the concept of the soliton and inverse scattering theory. Since then, many numerical

*Correspondence to: Takayuki Utsumi, Electronics and Computer Science, Tokyo University of Science, Yamaguchi, 1-1 Daigaku-dori, Sanyou-Onoda, Yamaguchi, 756-0884, Japan. Email: utsumi@ed.yama.tus.ac.jp

methods have been proposed to elucidate complicated processes by accurately solving the nonlinear partial differential equations (PDEs). The methods belong essentially to one of two classes: spectral methods and grid methods. The main difference between these two methods comes from the methodology in treating the spatial derivatives. With a spectral method the solution is approximated by some finite linear combination of differentiable basis functions, each one of which satisfies the boundary conditions. The derivatives in a spectral method do not suffer from numerical inaccuracies. With a grid method, such as the finite element method or the finite difference method, the derivatives are approximated by some differences. It is often difficult to approximate the derivatives with sufficient accuracy, because the derivatives are estimated by using only the values of the function on a compact set of grid points. In general, spectral methods give accurate solutions with a minimum number of discretization points, only if appropriate problem specific basis functions are applicable. However, a finite difference method is typically more flexible and easier to implement than a spectral method for systems with complex boundary conditions. By considering the merits and demerits of each method, it is believed that the method in which the solution is expanded by a finite number of local differentiable basis functions is to be preferred.

As far as incorporating only the values at grid points, it seems difficult to improve grid methods which exemplify the spectral method's accuracy. Recently, a new numerical method, the CIP-Basis Set (CIP-BS) method [2–4], has been proposed by generalizing the concept of the Constrained Interpolation Profile (CIP) method [5, 6] from the viewpoint of the basis set. The idea of the CIP method is that not only values but also their first derivatives are treated as independent variables associated with the grid points, and the information lost inside the grid cell is retrieved by a Hermite type interpolation function [7]. The CIP method has been successfully applied to various complex linear and nonlinear hydrodynamic problems, covering both compressible and incompressible flow [8], such as shock wave generation, laser-induced evaporation, and elastic-plastic flow. However, the methods using matrix operations are advantageous in investigating the characteristics of the system, and a number of numerical methods for large, sparse systems developed for the finite difference method or the finite element method can be adopted. With this view, the CIP-BS method has introduced a polynomial basis set, by which physical quantities are approximated with their values and derivatives associated with grid points. The governing equations are discretized into matrix form equations requiring the residuals to be orthogonal to the basis functions via the same principle as the Galerkin method. The CIP-BS method, in which the local polynomial basis functions corresponding to the values and spatial derivatives at each grid point belong to the complete set and the class C^K , is called the CIP-BS^K method. Numerical results in the solution of the linear Schrödinger equation have demonstrated that accurate solutions are obtained by the method and that the use of a higher order basis set is essential in increasing accuracy.

The purpose of this paper is to show that the CIP-BS method can be extended for nonlinear operations on functions in the framework of differential algebra, and can be a universal solver of nonlinear PDEs by exemplifying the solutions of the one-dimensional

coupled nonlinear Schrödinger (CNLS) equations for the collision of two solitary waves:

$$i\partial_t u + \partial_x^2 u + (|u|^2 + \beta|v|^2)u = 0, \quad (1.1a)$$

$$i\partial_t v + \partial_x^2 v + (|v|^2 + \beta|u|^2)v = 0, \quad (1.1b)$$

where u and v are complex functions, and β is a coupling constant. Since the CNLS equations describe the propagation of light waves in a nonlinear birefringent optical fiber, they have been studied intensively over 30 years to realize the idea of using optical solitons as information bits in high-speed telecommunication systems. Moreover, collision of solitary waves is a common phenomena in science and engineering. They have diverse applications in many areas of physics, including nonlinear optics, hydrodynamics, and plasma physics.

The paper is organized as follows: In Section 2, we briefly review the CIP-BS method, adding extensions to adapt the method to nonlinear PDEs. In Section 3, the discretized equations are explicitly described for the CNLS equations. In Section 4, the efficiency and accuracy of the CIP-BS method are demonstrated through the numerical results for the interaction of solitons. The fact that the boundary conditions are imposed in a simple manner with one-to-one correspondence to the analytical one is also shown. Concluding remarks are given in Section 5.

2 Numerical method

Since the CIP-BS method is new and not widely known, we first summarize the method, adding extensions for applying it to nonlinear PDEs.

We need a basis set where it is easy to define values and derivatives of an arbitrary function, $f(x)$, at the grid points. Therefore, we assume that the functions in the one-dimensional domain R^1 can be approximated by the CIP-basis set of degree K method (CIP-BS ^{K}), where K refers to the order of the derivatives we retain in the calculation, through the expression

$$f(x) = \sum_{i=1}^N \sum_{k=0}^K f_i^{(k)} \phi_{k,i}(x), \quad (2.1)$$

where $f_i^{(k)}$ is the k -th coefficient at the grid point x_i , the summation with respect to the index i is taken over all grid points, and the basis functions, $\phi_{k,i}(x)$, on the local support $[x_{i-1}, x_{i+1}]$ are expressed in the form

$$\phi_{k,i}(x) = \theta_{i-1,i}(x)\phi_{k,i-}(x) + \theta_{i,i+1}(x)\phi_{k,i+}(x), \quad (2.2)$$

where $\theta_{i,i+1}(x) = \theta(x - x_i) - \theta(x - x_{i+1})$, with $\theta(x)$ denoting the Heaviside step function, and $\phi_{k,i-}(x)$, $\phi_{k,i+}(x)$ are polynomials of degree $(2K + 1)$ determined from the constraints:

$$D_x^l \phi_{k,i\pm}(x_i) = \begin{cases} 1 & \text{for } l = k \\ 0 & \text{for } l = 0, 1, \dots, k-1, k+1, \dots, K \end{cases} \quad (2.3)$$

$$D_x^l \phi_{k,i\pm}(x_{i\pm 1}) = 0 \quad \text{for } l = 0, 1, \dots, K, \tag{2.4}$$

where $D_x = \partial_x$ is the derivative operator in x , and $D_x^0 = 1$. From these conditions, $\phi_{k,i-}(x)$ and $\phi_{k,i+}(x)$ take the form $(c_0 + c_1x + \dots + c_Kx^K)(x - x_{i\pm 1})^{K+1}$, where c_i are constants determined from the $(K + 1)$ constraints of Eq.(2.3).

The first derivative of the basis function is expressed as

$$D_x \phi_{k,i}(x) = \theta_{i-1,i} D_x \phi_{k,i-}(x) + \theta_{i,i+1} D_x \phi_{k,i+}(x). \tag{2.5}$$

Here, we have used the fact that $\phi_{k,i\pm}(x)\delta(x - x_{i\pm 1}) = 0$ due to the relation $x\delta(x) = 0$, and $\phi_{k,i-}(x_i) = \phi_{k,i+}(x_i)$, where $\delta(x)$ is the Dirac delta function. Similarly, we can obtain the l -th order derivatives of $\phi_{k,i}(x)$ for $l \leq K + 1$ as

$$D_x^l \phi_{k,i}(x) = \theta_{i-1,i} D_x^l \phi_{k,i-}(x) + \theta_{i,i+1} D_x^l \phi_{k,i+}(x). \tag{2.6}$$

Although the basis functions are constructed by using the distribution function $\theta(x)$, the functions represented in the CIP-BS^K method belong to the class C^K . Therefore, it is easily found that the k -th spatial derivative of $f(x)$ at the grid point x_i equals the coefficient $f_i^{(k)}$, i.e.,

$$D_x^k f(x)|_{x=x_i} = f_i^{(k)}. \tag{2.7}$$

We can say that the basis set belongs to a complete set in the sense that the expansion (2.1) could represent the exact solution with any degree of accuracy in the limit $N \rightarrow \infty$ or $K \rightarrow \infty$. If $f(x) = 0$ in Eq.(2.1), we can deduce that all the coefficients $f_i^{(k)}$ are zero, and that the basis functions are linearly independent. Then the function $f(x)$ can also be represented by this basis set as $\mathbf{f} = (\mathbf{f}_1, \mathbf{f}_2, \dots, \mathbf{f}_N)$, where $\mathbf{f}_i = (f_i^{(0)}, f_i^{(1)}, \dots, f_i^{(K)})$.

Let us define addition and multiplication of the functions as follows:

$$f(x) + g(x) \Leftrightarrow \mathbf{f} + \mathbf{g} = (\mathbf{f}_1 + \mathbf{g}_1, \mathbf{f}_2 + \mathbf{g}_2, \dots, \mathbf{f}_N + \mathbf{g}_N) \tag{2.8}$$

$$cf(x) \Leftrightarrow c\mathbf{f} = (cf_1, cf_2, \dots, cf_N) \tag{2.9}$$

$$f(x)g(x) \Leftrightarrow \mathbf{f} \cdot \mathbf{g} = (\mathbf{f}_1 \cdot \mathbf{g}_1, \mathbf{f}_2 \cdot \mathbf{g}_2, \dots, \mathbf{f}_N \cdot \mathbf{g}_N), \tag{2.10}$$

where c is a scalar value. Addition and scalar multiplication for \mathbf{f}_i are

$$\mathbf{f}_i + \mathbf{g}_i = (f_i^{(0)} + g_i^{(0)}, f_i^{(1)} + g_i^{(1)}, \dots, f_i^{(K)} + g_i^{(K)}) \tag{2.11}$$

$$c\mathbf{f}_i = (cf_i^{(0)}, cf_i^{(1)}, \dots, cf_i^{(K)}) \tag{2.12}$$

and multiplication is given by

$$\mathbf{f}_i \cdot \mathbf{g}_i = (h_i^{(0)}, h_i^{(1)}, \dots, h_i^{(K)}), \tag{2.13}$$

where $h_i^{(j)} = \sum_{l=0}^j \frac{j!}{l!(j-l)!} f_i^{(l)} g_i^{(j-l)}$. The identity of addition and multiplication are $(0, 0, \dots)$ and $(1, 0, \dots)$, respectively. Eqs.(2.11) - (2.13) are the same as the definition for differential

algebra ${}_K D_1$, (see ref. [9]). Therefore, the nonlinear operation on a function $f(x)$, e.g., $f^{-1}(x)$, $\sqrt{f(x)}$, $\sin(f(x))$, or $\exp(f(x))$, can be represented by the basis set using the representation of $f(x)$. For example,

$$f^{-1}(x) = \left(\frac{1}{f_i^{(0)}}, -\frac{f_i^{(1)}}{f_i^{(0)2}}, \frac{2f_i^{(1)2} - f_i^{(0)} f_i^{(2)}}{f_i^{(0)3}} \right)$$

when $K = 2$ and $f_i^{(0)} \neq 0$. It is worth noting that, although the operation D_x^n maps ${}_K D_1$ into ${}_{K-n} D_1$ in the differential algebra, we represent D_x^n as a matrix by introducing the scalar product of the basis function $\phi_{k,i}(x)$ and $\phi_{k',i'}(x)$ in the domain R as (see [2]):

$$\langle \phi_{k,i} | \phi_{k',i'} \rangle \equiv \int_R \phi_{k,i}(x) \phi_{k',i'}(x) dx. \tag{2.14}$$

Time evolution PDEs $\partial f(x,t)/\partial t = \hat{L}[f(x,t)]$, where \hat{L} is a linear or nonlinear operator involving spatial derivatives only, are reduced to ordinary differential equations by the scalar product. Applying $\langle \phi_{k,i} | \bullet \rangle$, ($k = 0, 1, 2, \dots, K, i = 0, 1, 2, \dots, N$), to the left-hand side of the equation, we obtain

$$S \frac{d\mathbf{f}}{dt} = L[\mathbf{f}], \tag{2.15}$$

where S is a positive-definite matrix with the elements $S_{ki,k'i'} = \langle \phi_{k,i} | \phi_{k',i'} \rangle$, and L is a linear or nonlinear operator on \mathbf{f} . It is noted that, if the value of $f_{i_b}^{(k_b)}$ is specified as the boundary condition, the equation corresponding to the $\langle \phi_{k_b,i_b} |$ is not included in Eq.(2.15). Since $S_{ki,k'i'}$ is non-zero only for $i' = i - 1, i, i + 1$, S is a band diagonal matrix with bandwidth $3(K + 1)$. A term $D_x^{n_1} f(x,t) D_x^{n_2} f(x,t) \dots D_x^{n_m} f(x,t)$ in $L[f(x,t)]$ is transformed to

$$L_{ki,k_1 i_1, \dots, k_m i_m}^{(0n_1 n_2 \dots n_m)} f_{i_1}^{(k_1)} f_{i_2}^{(k_2)} \dots f_{i_m}^{(k_m)}, \tag{2.16}$$

where

$$L_{ki,k_1 i_1, \dots, k_m i_m}^{(0n_1 n_2 \dots n_m)} \equiv \langle \phi_{k,i} | D_x^{n_1} \phi_{k_1 i_1} \dots D_x^{n_m} \phi_{k_m i_m} \rangle,$$

and the summations for k_1, k_2, \dots are taken on $0, 1, \dots, K$, and those for i_1, i_2, \dots on the grid points. Hereafter, if a subscript appears twice in a term, this summation is assumed. For example, if L contains a nonlinear term $f \partial f / \partial x$, the element of the corresponding matrix is $L_{ki,k_1 i_1, k_2 i_2}^{(001)} = \langle \phi_{k,i} | \phi_{k_1 i_1} D_x \phi_{k_2 i_2} \rangle$. The elements of the matrix representation of the operator L are non-zero only for $i_l = i - 1, i, i + 1$, are symmetric for the interchange of the index $k_l i_l$ and $k_{l'} i_{l'}$ when $n_l = n_{l'}$, and can be analytically calculated. The rank of the differential operator must satisfy one of the following conditions:

- (1) $n_l \leq K$ for $l = 1, 2, \dots, m$;
- (2) the maximum of n_l is $K + 1$, and the other n_l are less than K ;
- (3) the maximum of n_l is $K + 2$, and the other n_l are less than $K - 1$.

Otherwise, terms like $\theta(x)\delta(x)'$, which cannot be regularized, would appear. This discretization procedure is equivalent to the one in the Galerkin method in which the residual $\frac{\partial}{\partial t}f(x, t) - L[f(x, t)]$ is required to be orthogonal to the basis functions $\phi_{\mathbf{k}, \mathbf{i}}(x)$.

Finally, we briefly describe how the multi-dimensional basis set is constructed. We need a basis set such that the multi-dimensional function expressed by

$$f(\mathbf{x}) = \sum_{\mathbf{i}=1}^{\mathbf{N}} \sum_{\mathbf{k}=0}^{\mathbf{K}} f_{\mathbf{i}}^{(\mathbf{k})} \phi_{\mathbf{k}, \mathbf{i}}(\mathbf{x}), \tag{2.17}$$

which satisfies $\frac{\partial^{\mathbf{k}}}{\partial \mathbf{x}^{\mathbf{k}}} f(\mathbf{x})|_{\mathbf{x}=\mathbf{x}_{\mathbf{i}}} = f_{\mathbf{i}}^{(\mathbf{k})}$, where $\mathbf{x} = (x_1, x_2, \dots, x_v)$, $\mathbf{i} = (i_1, i_2, \dots, i_v)$, $\mathbf{N} = (N_1, N_2, \dots, N_v)$, $\mathbf{k} = (k_1, k_2, \dots, k_v)$, and v is the dimension of the space. It is easily verified that the functions

$$\phi_{\mathbf{k}, \mathbf{i}}(\mathbf{x}) = \phi_{k_1, i_1}(x_1) \phi_{k_2, i_2}(x_2) \cdots \phi_{k_v, i_v}(x_v) \tag{2.18}$$

satisfy the requirements when Eqs.(2.2) and (2.3) are taken into account. Then, the multi-dimensional PDEs are discretized with the above mentioned procedure, if the integration range in the scalar product is extended to the multi-dimensional domain, R^v .

3 The discretized CNLS equations

The discretized CNLS equations are obtained by multiplying $\langle \phi_{\mathbf{k}, \mathbf{i}} |$ on the left-hand side to Eq.(1.1):

$$\begin{aligned} iS_{ki, k' i'} \frac{du_{i'}^{(k')}}{dt} &= -L_{ki, k_1 i_1}^{(02)} u_{i_1}^{(k_1)} - L_{ki, k_1 i_1, k_2 i_2}^{(000)} (|u_{i_1}^{(k_1)}|^2 + \beta |v_{i_1}^{(k_1)}|^2) u_{i_2}^{(k_2)}, \\ iS_{ki, k' i'} \frac{dv_{i'}^{(k')}}{dt} &= -L_{ki, k_1 i_1}^{(02)} v_{i_1}^{(k_1)} - L_{ki, k_1 i_1, k_2 i_2}^{(000)} (|v_{i_1}^{(k_1)}|^2 + \beta |u_{i_1}^{(k_1)}|^2) v_{i_2}^{(k_2)}, \end{aligned} \tag{3.1}$$

where the representations for $|u|^2$ and $|v|^2$ are obtained from those for u, v by applying differential algebra. The difference between the two expressions ($|u(x)|^2$ and $|u|^2(x)$) is $\mathcal{O}(\Delta x^{2K+2})$, because the values and derivatives up to K th order of both functions coincide at each grid point. Although it seems straightforward and accurate to discretize the term $|u|^2 v$ as $L_{ki, k_1 i_1, k_2 i_2, k_3 i_3}^{(0000)} \overline{u}_{i_1}^{(k_1)} u_{i_2}^{(k_2)} v_{i_3}^{(k_3)}$, where the overline denotes the complex conjugate, we have used simplified expressions $L_{ki, k_1 i_1, k_2 i_2}^{(000)} |u_{i_1}^{(k_1)}|^2 v_{i_2}^{(k_2)}$ to reduce the complexity of the code and the computational time.

The local norm $\mathcal{N}_u, \mathcal{N}_v$, momentum \mathcal{J} , and energy \mathcal{E} are conserved when integrated over x , *i.e.*,

$$\begin{aligned} \frac{d}{dt} \mathcal{N}_u &= \frac{d}{dt} \int_R \mathcal{N}_u dx = 0, & \frac{d}{dt} \mathcal{N}_v &= \frac{d}{dt} \int_R \mathcal{N}_v dx = 0, \\ \frac{d}{dt} \mathcal{J} &= \frac{d}{dt} \int_R \mathcal{J} dx = 0, & \frac{d}{dt} \mathcal{E} &= \frac{d}{dt} \int_R \mathcal{E} dx = 0, \end{aligned}$$

where

$$\begin{aligned} \mathcal{N}_u &= |u|^2, \mathcal{N}_v = |v|^2, \\ \mathcal{J} &= \mathcal{J}_u + \mathcal{J}_v = -\frac{i}{2}(\bar{u}\partial_x u - u\partial_x \bar{u}) - \frac{i}{2}(\bar{v}\partial_x v - v\partial_x \bar{v}), \\ \mathcal{E} &= \mathcal{E}_u + \mathcal{E}_v + \mathcal{E}_I = \frac{1}{2}|u|^4 - \partial_x \bar{u}\partial_x u + \frac{1}{2}|v|^4 - \partial_x \bar{v}\partial_x v + \beta|u|^2|v|^2. \end{aligned}$$

The discretized expressions for the global norm N_u, N_v , momentum J , and energy E are written as:

$$\begin{aligned} N_u &= L_{k_1 i_1, k_2 i_2}^{(00)} \bar{u}_{i_1}^{(k_1)} u_{i_2}^{(k_2)}, \quad N_v = L_{k_1 i_1, k_2 i_2}^{(00)} \bar{v}_{i_1}^{(k_1)} v_{i_2}^{(k_2)}, \\ J &= -\frac{i}{2} L_{k_1 i_1, k_2 i_2}^{(01)} [(\bar{u}_{i_1}^{(k_1)} u_{i_2}^{(k_2)} - u_{i_1}^{(k_1)} \bar{u}_{i_2}^{(k_2)}) + (\bar{v}_{i_1}^{(k_1)} v_{i_2}^{(k_2)} - v_{i_1}^{(k_1)} \bar{v}_{i_2}^{(k_2)})], \\ E &= \frac{1}{2} L_{k_1 i_1, k_2 i_2}^{(00)} (|u_{i_1}^{(k_1)}|^2 |u_{i_2}^{(k_2)}|^2 + |v_{i_1}^{(k_1)}|^2 |v_{i_2}^{(k_2)}|^2) - L_{k_1 i_1, k_2 i_2}^{(11)} (\bar{u}_{i_1}^{(k_1)} u_{i_2}^{(k_2)} + \bar{v}_{i_1}^{(k_1)} v_{i_2}^{(k_2)}) \\ &\quad + \beta L_{k_1 i_1, k_2 i_2}^{(00)} |u_{i_1}^{(k_1)}|^2 |v_{i_2}^{(k_2)}|^2, \end{aligned}$$

where $L_{k_i, k'_i i'_i}^{(11)} = \langle D_x \phi_{k,i} | D_x \phi_{k'_i i'_i} \rangle$.

We emphasize that the above discretized CNLS equations can also be derived with the Lagrangian formalism regarding $u_i^{(k)}, \bar{u}_i^{(k)}, v_i^{(k)}, \bar{v}_i^{(k)}$ as independent variables. By substituting the expansions (2.1) for u, v into the Lagrangian

$$\begin{aligned} L(t) &= \int_R \left[\frac{i}{2} (u\partial_t \bar{u} - \bar{u}\partial_t u) + \partial_x \bar{u}\partial_x u - \frac{1}{2}|u|^4 \right. \\ &\quad \left. + \frac{i}{2} (v\partial_t \bar{v} - \bar{v}\partial_t v) + \partial_x \bar{v}\partial_x v - \frac{1}{2}|v|^4 - \beta|u|^2|v|^2 \right] dx, \end{aligned} \tag{3.2}$$

the Euler equations yield

$$\begin{aligned} iS_{k_i, k'_i i'_i} \frac{du_{i'}^{(k')}}{dt} &= -L_{k_i, k_1 i_1}^{(02)} u_{i_1}^{(k_1)} - L_{k_i, k_1 i_1, k_2 i_2, k_3 i_3}^{(0000)} (\bar{u}_{i_1}^{(k_1)} u_{i_2}^{(k_2)} + \beta \bar{v}_{i_1}^{(k_1)} v_{i_2}^{(k_2)}) u_{i_3}^{(k_3)}, \\ iS_{k_i, k'_i i'_i} \frac{dv_{i'}^{(k')}}{dt} &= -L_{k_i, k_1 i_1}^{(02)} v_{i_1}^{(k_1)} - L_{k_i, k_1 i_1, k_2 i_2, k_3 i_3}^{(0000)} (\bar{v}_{i_1}^{(k_1)} v_{i_2}^{(k_2)} + \beta \bar{u}_{i_1}^{(k_1)} u_{i_2}^{(k_2)}) v_{i_3}^{(k_3)}, \end{aligned} \tag{3.3}$$

and their complex conjugate equations. Here, we have used the symmetry property of L . After making above mentioned approximations, we obtain Eq.(3.1). In this derivation, the discretized Lagrangian is a function of the amplitudes of the modes $q(t)$ and $\dot{q}(t)$ ($q = u_i^{(k)}, \bar{u}_i^{(k)}, v_i^{(k)}, \bar{v}_i^{(k)}$). The dynamics can be discussed in the same manner as in ordinary mechanics.

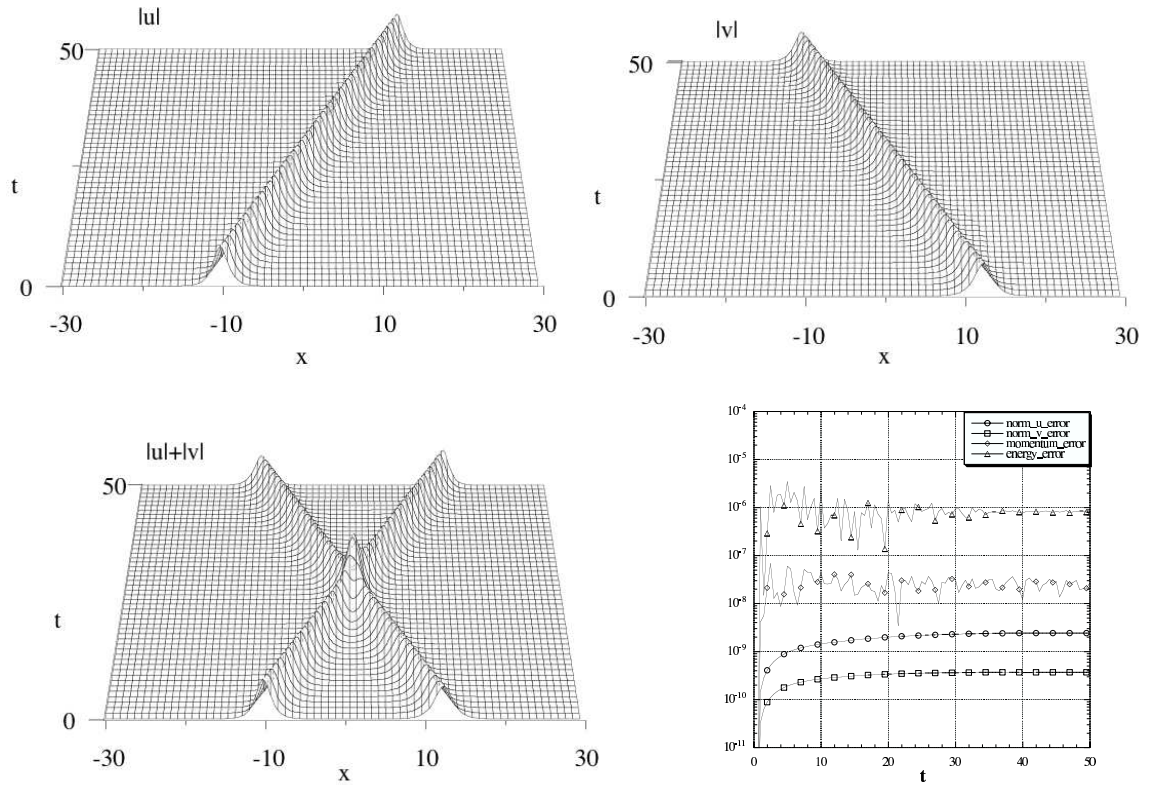


Figure 1: The solutions of the CNLS equations for the interaction of two solitons with $\beta = 0, v_0 = 1.0$, and $d_0 = 25$. The surface plots show the amplitude of the solitons. The line plot shows the absolute errors of the global norm, momentum, and energy, where the first calculated values are taken as a reference, $N_u(0) = 4.8, N_v(0) = 4.0, J(0) = 0.2$, and $E(0) = 3.0873$.

4 Numerical results

We consider the CNLS equations (1.1) with the initial conditions [12, 13]

$$\begin{aligned}
 u(x, 0) &= \sqrt{2}r_1 \operatorname{sech}(r_1x - \xi_1)e^{iv_1x}, \\
 v(x, 0) &= \sqrt{2}r_2 \operatorname{sech}(r_2x - \xi_2)e^{iv_2x}.
 \end{aligned}$$

In our calculations, we take $r_1 = 1.2, r_2 = 1, \xi_1 = -\xi_2 = d_0/2$, and $v_1 = -v_2 = -v_0/4 > 0$ such that the two solitons with different amplitudes approach with the velocity v_0 and collide at $x \approx d_0(\frac{1}{r_2} - \frac{1}{r_1})/4 \approx 0$ after $t \approx \frac{1}{2}(\frac{1}{r_1} + \frac{1}{r_2})d_0/v_0 \approx d_0/v_0$. In the computer program, a uniform grid is used and the matrix elements of S and L are calculated analytically. Since in many cases, the discretized equations (2.15) are stiff, the implicit solver with general sparse Jacobian matrices developed by Hindmarsh [10] (*dlsodis* routine) is used to time marching the discretized equations by requiring an overall tolerance level of $\varepsilon = 10^{-10}$.

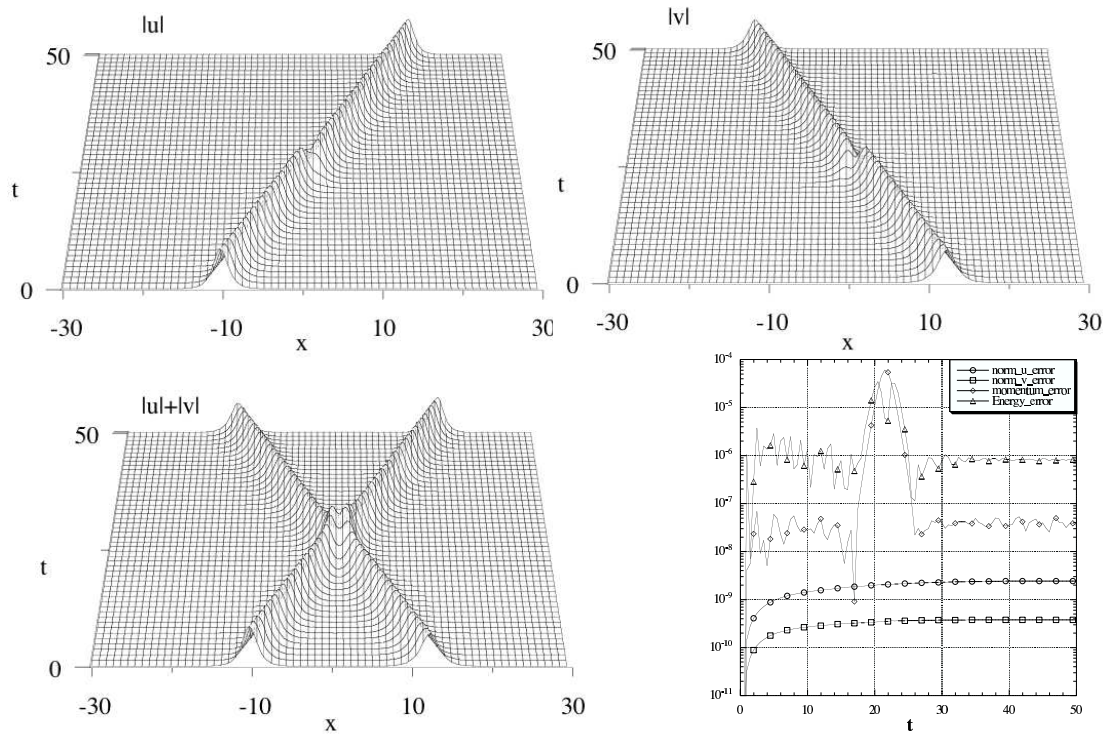


Figure 2: The solutions of the CNLS equation for the interaction of two solitons with $\beta = 1, v_0 = 1.0,$ and $d_0 = 25$. The surface plots show the amplitude of the solitons. The line plot shows the absolute errors of the global norm, momentum, and energy, where the first calculated values are taken as a reference, $N_u(0) = 4.8, N_{v(0)} = 4.0, J(0) = 0.2,$ and $E(0) = 3.0873$.

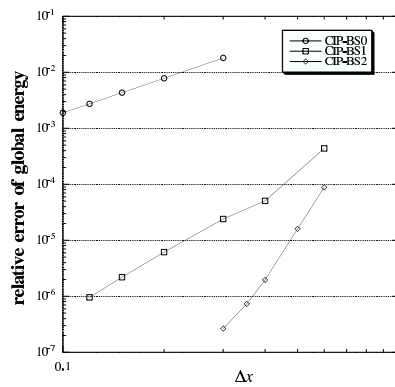


Figure 3: The relative errors of the global energy at $t = 50$ versus the grid interval for the solution of the CNLS equations for the interaction of two solitons with $\beta = 1, v_0 = 1.0,$ and $d_0 = 25$. The analytical value is taken as a reference. The orders of the CIP-BS method used are as indicated.

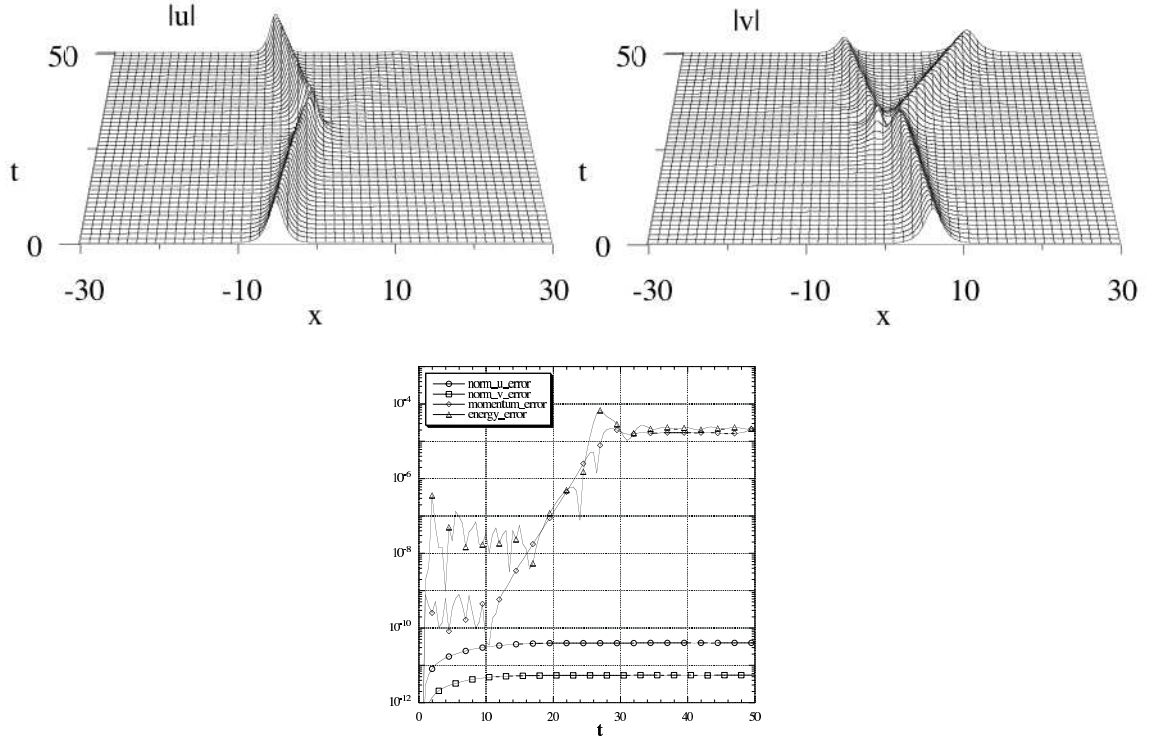


Figure 4: The solutions of the CNLS equations for the interaction of two solitons with $\beta = 2/3, v_0 = 0.32$ and, $d_0 = 12.5$. The surface plots show the amplitude of the solitons. The line plot shows the absolute errors of the global norm, momentum, and energy, where the first calculated values are taken as a reference $N_u(0) = 4.8, N_v(0) = 4.0, J(0) = 0.064$, and $E(0) = 3.581$.

Figs. 1 and 2 show the results for $\beta = 0, v_0 = 1.0, d_0 = 25$ and $\beta = 1, v_0 = 1.0, d_0 = 25$, respectively. Since the CNLS equations for $\beta = 0$ reduce to two independent NLS equations, and for $\beta = 1$ to the Manakov equation, the behaviors of the solitons are completely known from exact inverse scattering solutions [14]. The computations are carried out over the range $-30 \leq x \leq 30, 0 \leq t \leq 50$ with a time step $\Delta t = 0.01$ and a space interval $\Delta x = 0.3$ by the CIP-BS¹ method. From Fig. 1, we can see the two solitons move independently as expected by the analytic solution [12], $\sqrt{2}r_i \text{sech}(r_i x - 2r_i v_i t - \xi_i) e^{i(v_1 x + (r_i^2 - v_i^2)t)}$ for $i = 1, 2$. From Fig. 2, we can observe that the solitons collide at $t \approx 23$ and retain their identity after nonlinear interactions with the other soliton. The errors of the global norm N_u, N_v , momentum J , and energy E are also shown in this figure. Although it seems that the errors of the momentum and energy increase during strong interaction, it is only due to the lack of approximation accuracy for monitoring variables, *i.e.* the error is reduced soon after the interaction ended. The conservation property of the energy by the CIP-BS method is well compared with those in [13], in which the multi-symplectic method is used. The relative errors of the global energy versus Δx and K , for the case $\beta = 1, v_0 = 1.0, d_0 = 25$ and at the end of computation, are plotted in Fig. 3. From this figure, we can recognize the CIP-BS⁰, CIP-BS¹ and CIP-BS² methods have

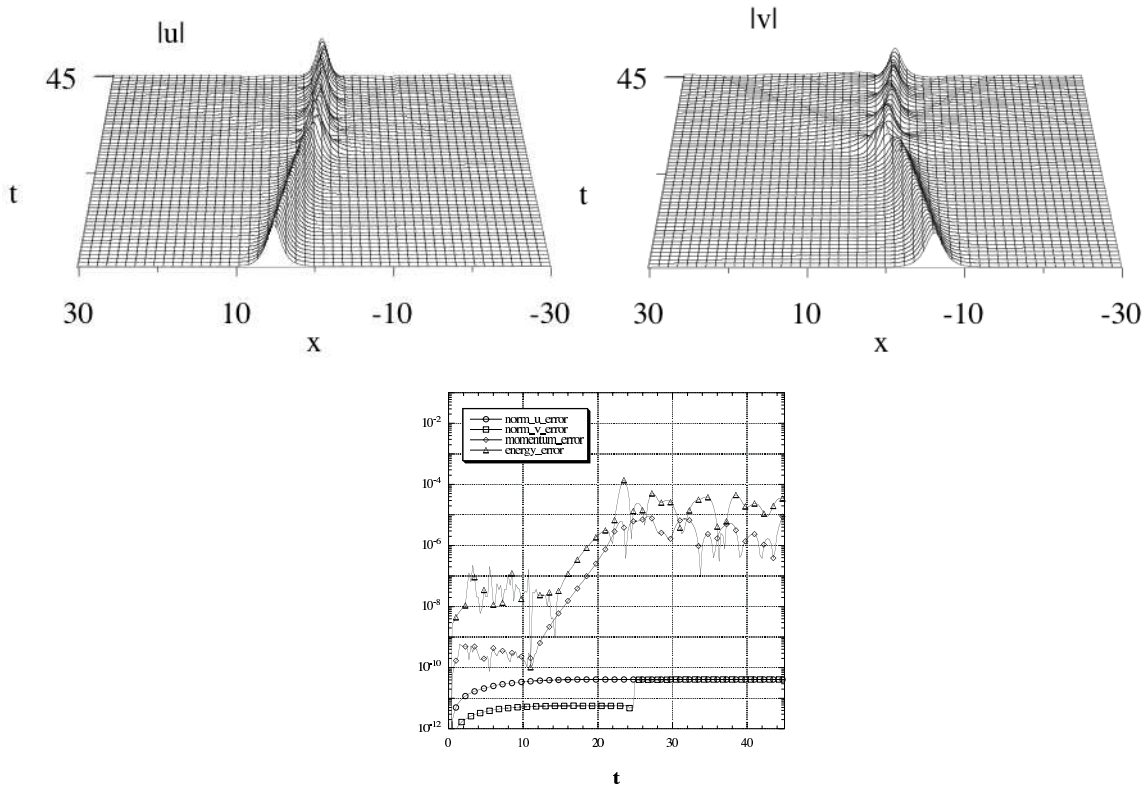


Figure 5: The solutions of the CNLS equations for the interaction of two solitons with $\beta = 0.3$, $v_0 = 0.4$, and $d_0 = 12.5$. The surface plots show the amplitude of the solitons. The line plot shows the absolute errors of the global norm, momentum, and energy, where the first calculated values are taken as a reference $N_u(0) = 4.8$, $N_v(0) = 4.0$, $J(0) = 0.08$, and $E(0) = 3.549$.

roughly 2nd, 4th and 6th order, *i.e.* order $2K + 2$, accuracy despite nonlinear interactions. Although in this paper we only show numerical results calculated by the CIP-BS¹ method, the solutions are quickly improved by increasing the number of grid points, N , and/or the order of the method, K .

Fig. 4 shows the results for the interaction of two solitons with $\beta = 2/3$, $v_0 = 0.32$, $d_0 = 12.5$. The computation is done for $-70 \leq x \leq 70$ ($-30 \leq x \leq 30$ is shown in the figure), $0 \leq t \leq 50$ with a time step $\Delta t = 0.01$ and a space interval $\Delta x = 0.2$ by the CIP-BS¹ method. The computational errors of the global momentum and energy increase during interaction, and do not decrease. This is in contrary to the $\beta = 1$ case. We can say that the global norms are conserved well due to their small errors. For $\beta = 2/3$, the CNLS equations represent real single-mode birefringent fibers, where u and v represent the two-linear polarizations. Much theoretical and numerical work has been performed [12, 15–17] for the use of solitons as information bits in optical communication systems proposed by Hasegawa [18]. From Fig. 4 we observe that the collision takes place at $t \approx 26$. This is earlier than the expected time $t \approx 36$, because the two solitons collide with sharp angle and substantial interaction begins at $t \approx 10$. The right-moving soliton, which has larger

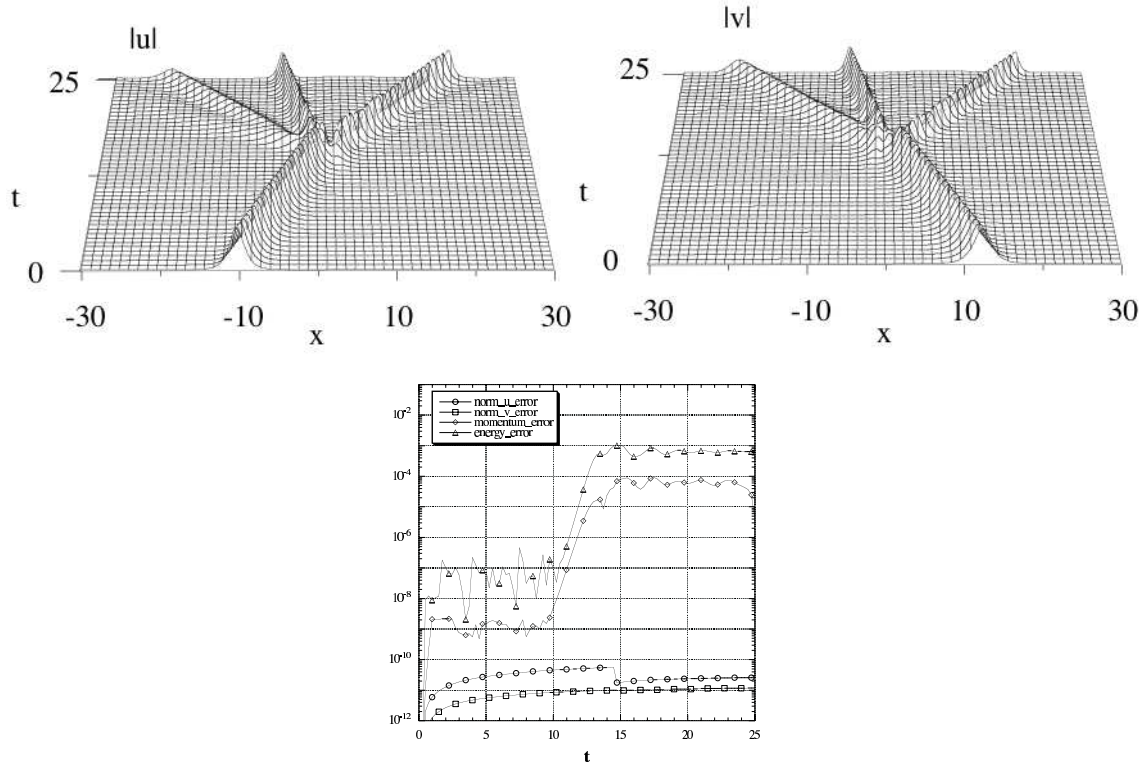


Figure 6: The solutions of the CNLS equations for the interaction of two solitons with $\beta = 3, v_0 = 1.6,$ and $d_0 = 25.$ The surface plots show the amplitude of the solitons. The line plot shows the absolute errors of the global norm, momentum, and energy, where the first calculated values are taken as a reference $N_u(0) = 4.8, N_v(0) = 4.0, J(0) = 0.32,$ and $E(0) = 2.229.$

momentum and energy, is reflected back by the collision and the amplitude becomes even larger. On the other hand, the left-moving soliton is reflected after collision, but becomes even smaller transferring its energy to the larger one. The evolution of the solitons depicted in Fig. 4 reproduces well the reflection scenario analyzed by the perturbation theory [12].

Figs. 5 and 6 show the results for the interaction of two solitons with $\beta = 0.3, v_0 = 0.4, d_0 = 12.5,$ and $\beta = 3, v_0 = 1.6, d_0 = 25,$ respectively. The computation is done for $-70 \leq x \leq 70$ ($-30 \leq x \leq 30$ is shown in the figure) with a time step $\Delta t = 0.01$ and a space interval $\Delta x = 0.2$ by the CIP-BS¹ method. The computational errors of the global momentum and energy increase from the beginning of the interaction, however, the global norms retain its accuracy well. The collision for β not close to 1 transcends analytical or perturbative treatments. However, interesting nonlinear phenomena like fusion and creation of a new vector soliton are expected for β values far away from 1. In Fig. 5 we can observe the fusion of two solitons colliding with small β and slow velocity. From Fig. 6 we can see that a new vector soliton is created after the collision of the two solitons with large β and moderate velocity which is chosen to attain an appropriate interaction time. Our results confirm previous research [12, 13] with high numerical accuracy.

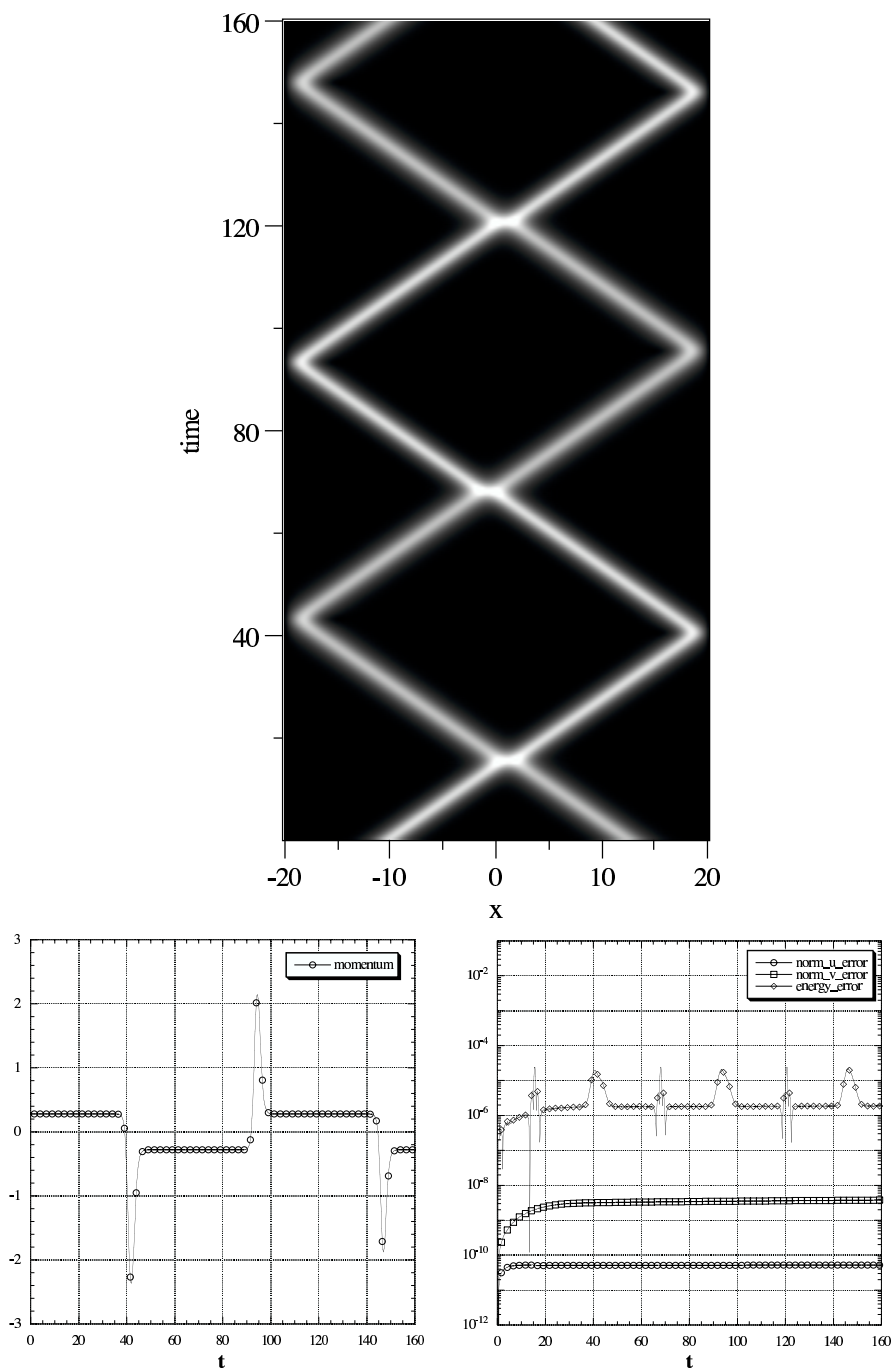


Figure 7: The bouncing of the two interacting solitons with $\beta = 1$, $v_0 = 1.4$, and $d_0 = 25$. The line plots show the time evolution of the global momentum and the absolute errors of the global norm and energy, where the first calculated values are taken as a reference $N_u(0) = 4.8$, $N_v(0) = 4.0$, and $E(0) = 2.559$.

In the above simulations (for $\beta = 0, 1, 2/3, 0.3, 3$), we have taken a spatial range large enough such that small fractions of the scattered wave with high energy do not reach the computational boundaries within the temporal range. In other words, the method to implement boundary conditions is not considered, *i.e.*, $u^{(k)}, v^{(k)}$ at the boundary are regarded as state variables and time evolved. As a final illustration, we show how the reflecting boundary conditions are incorporated. Fig. 7 demonstrates the bouncing of two interacting solitons against walls with $\beta = 1, v_0 = 1.4$ and $d_0 = 25$. The computation is done for $0 \leq t \leq 160$, $-20 \leq x \leq 20$ with a time step $\Delta t = 0.01$ and a space interval $\Delta x = 0.2$ by the CIP-BS¹ method. The boundary conditions $\mathcal{J}_u(x_1) = \mathcal{J}_v(x_1) = 0$ and $\mathcal{J}_u(x_N) = \mathcal{J}_v(x_N) = 0$ are realized by setting $u_1^{(1)} = v_1^{(1)} = 0$ and $u_N^{(1)} = v_N^{(1)} = 0$, respectively. From Fig. 7, we observe the global momentum changes its sign at $t \approx 40, 90$ and 150 as expected, and the global norm and energy are calculated accurately.

5 Conclusions

We have generalized the CIP-BS method by introducing matrix representations and clarifying the relation with differential algebra to adapt it to nonlinear partial differential equations. The linear and nonlinear partial differential equations are reduced to ordinary differential equations for values and spatial derivatives at the grid points. It is successfully applied to the one-dimensional coupled nonlinear Schrödinger equation. It has been proved that the method gives stable, low diffusion, and accurate results. Since the method does not depend on the structure of the specific properties of the governing equations, *e.g.*, the conservative quantities or the symplectic structure, we can expect that perturbative effects to the CNLS equations or other nonlinear systems are simulated properly. Furthermore, since the matrices, S and L , are sparse and sufficient to be calculated only at the beginning of the simulation, the method is computationally efficient.

We believe the CIP-BS method is applicable for the study of the dynamics of a broad spectrum of complex physical and engineering problems.

Acknowledgments

The authors would like to thank Prof. T. Tajima and Dr. T. Kimura at the Japan Atomic Energy Agency for their valuable discussion and encouragement.

References

- [1] N. J. Zabusky and M. D. Kruskal, Interaction of "Solitons" in a collisionless plasma and the recurrence of initial states, *Phys. Rev. Lett.*, 15 (1965), 240-243.
- [2] T. Utsumi, T. Yabe, J. Koga, T. Aoki and M. Sekine, Accurate basis set by the CIP method for the solutions of the Schrödinger equation, *Comput. Phys. Commun.*, 157 (2004), 121-138.
- [3] T. Utsumi, and H. Kimura, Solutions of partial differential equations with the CIP-BS method, *JSME Int. J.*, B47 (2004), 761-767.

- [4] T. Utsumi, T. Yabe, T. Aoki, and J. Koga, Solutions of hyperbolic equations with the CIP-BS method, *JSME International Journal*, B47 (2004), 768-776.
- [5] T. Yabe and T. Aoki, A universal solver for hyperbolic equations by cubic-polynomial interpolation I. One-dimensional solver, *Comput. Phys. Commun.*, 66 (1991), 219-232.
- [6] T. Yabe, T. Ishikawa and P. Y. Wang, A universal solver for hyperbolic equations by cubic-polynomial interpolation II. Two- and three-dimensional solvers, *Comput. Phys. Commun.*, 66 (1991), 233-242.
- [7] Carl de Boor, *A Practical Guide to Splines*, Springer-Verlag, New York, 1978.
- [8] T. Yabe, F. Xiao and T. Utsumi, The constrained interpolation profile method for multiphase analysis, *J. Comput. Phys.*, 169 (2001), 556-593.
- [9] M. Berz, Arbitrary order description of arbitrary particle optical systems, *Nucl. Instrum. Meth. A*, 298 (1990), 426-440.
- [10] A. C. Hindmarsh, LSODE and LSODI, two new initial value ordinary differential equation solvers, *ACM-SIGNUM Newsletter*, 15 (1980), 10-11.
- [11] A. L. Islas and C. M. Schober, On the preservation of phase space structure under multi-symplectic discretization, *J. Comput. Phys.*, 197 (2004), 585-609.
- [12] J. Yang, Multisoliton perturbation theory for the Manakov equations and its applications to nonlinear optics, *Phys. Rev. E*, 59 (2004), 2393-2405.
- [13] J. Q. Sun, and M. Z. Qin, Multi-symplectic methods for the coupled 1D nonlinear Schrödinger system, *Comput. Phys. Commun.*, 155 (2003), 221-235.
- [14] M. J. Ablowitz and H. Segur, *Solitons and the Inverse Scattering Transform*, SIAM, Philadelphia, 1981.
- [15] N. F. Smyth and W. L. Kath, Radiative losses due to pulse interactions in birefringent nonlinear optical fibers, *Phys. Rev. E*, 63 (2001), 36614-36622.
- [16] T. Ueda, and W. L. Kath, Dynamics of coupled solitons in nonlinear optical fibers, *Phys. Rev. A*, 42 (1990), 563-571.
- [17] J. Yang, Interactions of vector solitons, *Phys. Rev. E*, 64 (2001), 26607-26622.
- [18] A. Hasegawa and F. Tappert, Transmission of stationary nonlinear optical pulses in dispersive dielectric fibers. I. Anomalous dispersion, *Appl. Phys. Lett.*, 23 (1973), 142-144.